Title

Postnatal Ablation of Synaptic Retinoic Acid Signaling Impairs Cortical Information Processing and Sensory Discrimination in Mice

Journal

Journal of Neuroscience, 38(23)

ISSN

0270-6474

Authors

Park, Esther
Tjia, Michelle
Zuo, Yi
et al.

Publication Date

2018-06-06

DOI

10.1523/jneurosci.3028-17.2018

Peer reviewed

Cellular/Molecular

Postnatal Ablation of Synaptic Retinoic Acid Signaling Impairs Cortical Information Processing and Sensory Discrimination in Mice

Esther Park,[1]* Michelle Tjia,[2]* Yi Zuo,[2] and Lu Chen[1]

[1]Departments of Neurosurgery, Neuropsychiatry and Behavioral Sciences, Stanford Neuroscience Institute, Stanford University School of Medicine, Stanford, California 94305-5453, and [2]Department of Molecular, Cell and Developmental Biology, University of California Santa Cruz, Santa Cruz, California 95064

Retinoic acid (RA) and its receptors (RARs) are well established essential transcriptional regulators during embryonic development. Recent findings in cultured neurons identified an independent and critical post-transcriptional role of RA and RARα in the homeostatic regulation of excitatory and inhibitory synaptic transmission in mature neurons. However, the functional relevance of synaptic RA signaling *in vivo* has not been established. Here, using somatosensory cortex as a model system and the RARα conditional knock-out mouse as a tool, we applied multiple genetic manipulations to delete RARα postnatally in specific populations of cortical neurons, and asked whether synaptic RA signaling observed in cultured neurons is involved in cortical information processing *in vivo*. Indeed, conditional ablation of RARα in mice via a CaMKIIα-Cre or a layer 5-Cre driver line or via somatosensory cortex-specific viral expression of Cre-recombinase impaired whisker-dependent texture discrimination, suggesting a critical requirement of RARα expression in L5 pyramidal neurons of somatosensory cortex for normal tactile sensory processing. Transcranial two-photon imaging revealed a significant increase in dendritic spine elimination on apical dendrites of somatosensory cortical layer 5 pyramidal neurons in these mice. Interestingly, the enhancement of spine elimination is whisker experience-dependent as whisker trimming rescued the spine elimination phenotype. Additionally, experiencing an enriched environment improved texture discrimination in RARα-deficient mice and reduced excessive spine pruning. Thus, RA signaling is essential for normal experience-dependent cortical circuit remodeling and sensory processing.

Key words: enriched environment; retinoic acid signaling; sensory deprivation; sensory discrimination; somatosensory cortex

Significance Statement

The importance of synaptic RA signaling has been demonstrated in *in vitro* studies. However, whether RA signaling mediated by RARα contributes to neural circuit functions *in vivo* remains largely unknown. In this study, using a RARα conditional knock-out mouse, we performed multiple regional/cell-type-specific manipulation of RARα expression in the postnatal brain, and show that RARα signaling contributes to normal whisker-dependent texture discrimination as well as regulating spine dynamics of apical dendrites from layer (L5) pyramidal neurons in S1. Deletion of RARα in excitatory neurons in the forebrain induces elevated spine elimination and impaired sensory discrimination. Our study provides novel insights into the role of RARα signaling in cortical processing and experience-dependent spine maturation.

Introduction

Retinoids are an essential nutrient for the development of the vertebrate CNS (Morriss-Kay and Sokolova, 1996; Janesick et al., 2015). Although retinal is important for photo-transduction in the retina, retinoic acid (RA) mediates virtually all other known functions of retinoids in the CNS. The most well known function of RA is transcriptional regulation of neurodevelopmental pro-

Received Oct. 20, 2017; revised April 28, 2018; accepted May 3, 2018.

Author contributions: E.P., M.T., Y.Z., and L.C. designed research; E.P. and M.T. performed research; E.P. contributed unpublished reagents/analytic tools; E.P. and M.T. analyzed data; M.T. and L.C. wrote the paper.

This work was supported by Grants from the National Institute of Mental Health (R01MH104227 and R01MH109475 to L.C., R01MH109475 and 1R01MH104227 to Y.Z.), Eunice Kennedy Shriver National Institute of Child Health and Human Development (R01HD084215 to L.C.), and National Institute of Neurological Disorders and Stroke (R01NS078791 to Y.Z.). We thank Drs. Kristin Arendt, Yu-Tien Hsu, and Ray Zhong for technical assistance and helpful discussions throughout the study, and Drs. Ju Lu and Jennifer Hodges for critical comments on this paper.

The authors declare no competing financial interests.

*E.P. and M.T. contributed equally to this work.

Correspondence should be addressed to either of the following: Dr. Lu Chen, Stanford University School of Medicine, 265 Campus Drive, G1034, Lorry Lokey Stem Cell Building, Stanford, CA 94305-5453, E-mail: luchen1@stanford.edu; or Yi Zuo, Department of Molecular, Cell and Developmental Biology, University of California Santa Cruz, 1156 High Street, Santa Cruz, CA 95064, E-mail: yizuo@ucsc.edu.

DOI:10.1523/JNEUROSCI.3028-17.2018

 0270-6474/18/385277-12$15.00/0

cesses, which is mediated by nuclear RA receptors (RARs; Mark et al., 2009).

In contrast to RA's well established roles in embryonic development, RA signaling in the adult brain is less understood. RA and RARα have been shown to regulate homeostatic synaptic plasticity in cultured hippocampal neurons (Maghsoodi et al., 2008; Sarti et al., 2013; Chen et al., 2014b). During normal excitatory synaptic transmission, RARα acts as a translational repressor through direct binding to substrate mRNAs and keeps them translationally dormant. During synaptic inactivity, the resulting reduction in dendritic calcium level triggers synthesis of RA (Wang et al., 2011; Arendt et al., 2015b), which in turn binds to RARα and reduces its affinity for mRNA, thus releasing the brake on substrate mRNA translation (Poon and Chen, 2008). One of the mRNAs regulated by RA signaling is the AMPA receptor (AMPAR) subunit GluA1 (Poon and Chen, 2008). De-repression of mRNA translation allows for dendritic protein synthesis (including GluA1) and insertion of GluA1-containing AMPAR subunits into the postsynaptic membrane, thus increasing the excitatory synaptic strength (Maghsoodi et al., 2008). A concomitant depression of inhibitory synaptic transmission by RA through a protein synthesis-dependent mechanism has also been described (Sarti et al., 2013). Thus, RA rapidly readjusts the balance of synaptic excitation/inhibition in response to synaptic silencing. Although initially described in the context of homeostatic plasticity, RA's potential impact on Hebbian synaptic plasticity is now also beginning to emerge (Arendt et al., 2015a). Together, these *in vitro* studies suggest that synaptic signaling mediated by RA and RARα may impact synaptic plasticity beyond homeostatic synaptic regulation (Yee et al., 2017). Whether and how synaptic RA signaling mediated by RARα impacts function of a neural circuit *in vivo*, however, remains largely unknown.

More than 90% of excitatory synapses in the mammalian brain are formed on dendritic spines (Gray, 1959). As the receiving side of synaptic inputs, dendritic spines contain the molecular components necessary for synaptic signaling and plasticity in the postsynaptic compartment; these include neurotransmitter receptors, postsynaptic scaffold proteins, cytoskeletal and adaptor proteins, and various signaling molecules (Nimchinsky et al., 2002; Sheng and Kim, 2011; Colgan and Yasuda, 2014). Spine morphology and density vary among neuronal types, across developmental stages, and in response to experiences such as sensory manipulation, environmental enrichment (EE), and learning (Nimchinsky et al., 2002; Konur et al., 2003; Lee et al., 2007; Chen et al., 2015; Zhou et al., 2017). In the past 2 decades, live imaging studies have revealed a dynamic picture of spine formation and elimination, as well as their morphological changes (Holtmaat and Svoboda, 2009; Fu and Zuo, 2011; Chen and Nedivi, 2013; Chen et al., 2014a). Achieved through postsynaptic receptor trafficking in and out of the synaptic membrane, multiple forms of long-term synaptic plasticity involve changes of postsynaptic neurotransmitter receptor abundance (Huganir and Nicoll, 2013), which has been shown to correlate with sizes of spines (Hering and Sheng, 2001). Because RA signaling modulates local translation of synaptic proteins and affects synaptic strength (Maghsoodi et al., 2008; Poon and Chen, 2008), it is conceivable that its impact at synapses may also manifest as changes in spine morphology and dynamics.

In this study, we investigated the role of RA signaling in cortical circuits. Using RARα conditional knock-out mice (Chapellier et al., 2002; Sarti et al., 2012) for regional/cell-type-specific deletion of RARα in the postnatal brain, we found that expression of RARα in postnatal S1 excitatory neurons is required for normal whisker-dependent texture discrimination. Deletion of RARα in all forebrain excitatory neurons not only impairs somatosensory processing at the behavioral level, but also elevates spine elimination on apical dendrites from layer (L)5 pyramidal neurons (PNs) in S1. Interestingly, the increase in spine elimination required normal whisker sensory inputs. Additionally, enhanced sensory experience with an EE reverses excessive spine elimination and rescues texture discrimination in the mutant mice. These data suggest that RARα signaling participates in multifaceted synaptic remodeling in response to sensory experiences and influences cortical function.

Materials and Methods

Mice

Postnatal day (P)27–P38 male and female littermates were used for this study. Breeding colonies were maintained and animal experiments were performed following protocols approved by Administrative Panel on Laboratory Animal Care at Stanford University and University of California Santa Cruz. Mice were group-housed with littermates and maintained under a 12 h daylight cycle. The RARα$^{fl/fl}$ mice (C57BL/6 background) were a generous gift from Dr. Pierre Cambon and Norbert Ghyselinck (IGBNC, Stasbourg, France; Chapellier et al., 2002). These mice were crossed to the Thy1-YFP-H line (stock 003782, The Jackson Laboratory) and an additional cross to either CaMKIIα-Cre (Tsien et al., 1996; B6.Cg-Tg(CaMKIIα-Cre)T29-1Stl/J; The Jackson Laboratory) or Rbp4-Cre (GENSAT; RRID:MMRRC_031125-UCD; Gerfen et al., 2013) driver mice to obtain yellow fluorescent protein (YFP)-expressing conditional KO mice.

Stereotaxic surgery

Stereotaxic injections were performed on P0–P3 male and female RARα$^{fl/fl}$ pups. Purified AAV-DJ viruses expressing GFP-tagged active Cre or truncated-inactive Cre recombinase (mCre) driven by a synapsin promoter (Kaeser et al., 2011) were injected into either S1 or visual cortex (V1). Pups were anesthetized by hypothermia for 3 min, and placed in a clay mold to position and fix the head below the stereotaxic apparatus. The stereotaxic frame was aligned with the pups at bregma using visual landmarks and 20 nl of adeno-associated viruses (AAVs) were injected. Using the center of bregma to zero the x (anterior–posterior) and y (medial–lateral) coordinates, and the skin surface to zero the z (depth) coordinate, the injection coordinates were (x, y, z in mm): S1 ($\pm$1.6, 1.5, $-$0.75) and V1 ($\pm$1.3, 0.5, $-$0.75). Mice were recovered on a heated pad and returned to their home cages when ambulatory.

Histology

To verify sites of viral injection following behavioral studies, mice were perfused with 4% paraformaldehyde in PBS and incubated in 30% sucrose and 4% paraformaldehyde in PBS overnight. Coronal sections and tangential sections of S1 were made to observe the barrels at different angles. Tangential sections were cut as previously described (Welker and Woolsey, 1974). S1 was dissected and placed between two slide glasses with 1.2 mm spacers in 4% paraformaldehyde solution overnight. The brains were then sliced with a cryostat into 50 μm coronal or tangential sections. For visualization of barrels in S1, 50 μm brain slices were incubated with cytochrome c solution [0.008% cytochrome c (Sigma-Aldrich, type III, C-2506), 0.05% diaminobenzidine tetrachloride, 4% sucrose, and 100 mM sodium phosphate buffer, pH 7.4] overnight at 4°C. The slices were washed with PBS three times for 10 min and mounted on slides with Vectashield containing DAPI (Vector Laboratories). Images of 3–4 slices were taken per animal. Three animals were analyzed for each genotype. Images were acquired using an Olympus BX61US microscope with Olympus UPlanSAPO 10× objective. Area of the barrels in the tangential sections were analyzed by outlining the barrels in NIH ImageJ software (RRID:SCR_003070) and measuring the area of barrels and septa.

Single-cell RT-qPCR

Single cells and mRNA were amplified using the protocol previously described (Földy et al., 2016). Acute slices were obtained from P30 mice and single pyramidal cells were extracted from the somatosensory cortex

L5. Cell extract volume was minimized to 1 μl. mRNA obtained from the extracts were amplified using Superscript III One-Step RT-PCR System with Platinum Taq High Fidelity DNA polymerase (Invitrogen, catalog #12574035). RT-qPCR was then performed using TaqMan Gene Expression Master Mix (Applied Biosystems, catalog #4369016) with TaqMan primers from Life Technologies; RARα (Mm00436262_m1), actinβ (Mm02619580_g1), GFAP (Mm01253033_m1), and Rbfox3 (Mm01248771_m1). Actin was the endogenous control. RbFox3 was used as a neuronal marker and GFAP was used as a glial cell marker. Those cells expressing GFAP were excluded from the sample. The number of cells per animal (5–8 cells per animal) was averaged and compared across three animals.

Behavior

Open field test. Mice were placed in a 40 (L) × 40 (W) × 40 cm (H) open-field chamber. Locomotor activity was recorded for 30 min using an overhead digital camera and tracked using Viewer III tracking system (BioServe). Time spent in the center was measured by a 10 × 10 cm area in the center.

Texture preference test. Mice were habituated in the testing chamber [40 (L) × 40 (W) × 40 cm (H) open-field chamber] for 30 min on the first day. The next day, the mice were presented with two different textures for 5 min in the testing chamber. Textures were present on 50 ml conical tubes wrapped with the corresponding sandpaper grains (220, 320, or 400 grit). The roughest sandpaper grain is 220 grit and the smoothest is 400 grit. Smooth texture (SM) is 220 grit wrapped with cellophane so that it has a similar visual appearance to 220 grit but with a completely smooth texture. The other three textures (400, 320, and 200 grit) were chosen also based on their very similar visual appearance (i.e., color) of the grains. The conical tubes were weighted down with 50 ml of water. The time of the nose spent within 2 cm perimeter of each texture was recorded using an overhead digital camera and tracked using Viewer III tracking system (BioServe).

Novel texture discrimination test. Mice were habituated in the above-mentioned testing chamber for 30 min on the first day. On the second day, mice were presented with two columns with identical textures for 5 min in the testing chamber and then placed in a holding cage for 5 min. For the test phase, both columns were replaced; one with the same texture presented before and the other with a novel texture, and the mice explored the chamber freely for 5 min. The time of the nose spent within 2 cm perimeter of each texture was recorded using an overhead digital camera and tracked using Viewer III tracking system (BioServe). Discrimination of novel texture was quantified as percentage of time spent on each texture as well as discrimination ratio (time spent on novel texture/time spent on familiar texture).

Novel object discrimination test. Mice were habituated in the above testing chamber for 30 min on the first day. For the trial phase starting the next day, mice were presented with two identical objects (identical Lego pieces) for 10 min and then placed in a holding cage for 5 min. For the test phase, one of the objects was replaced with a novel object (Lego pieces with different shapes and colors) and the mice were allowed to explore the chamber freely for 10 min. The time of the nose spent within 2 cm perimeter of each object was recorded using an overhead digital camera and tracked using Viewer III tracking system (BioServe). Discrimination of novel object was quantified as percentage of time spent on each object as well as discrimination ratio (time spent on novel object/time spent on familiar object).

Y-maze task. A plastic Y maze (Stoelting) was used to measure spatial working memory indicated by the percentage of spontaneous alternation of arm exploration. Individual mice were placed in the center of the Y maze and allowed to freely explore for 5 min. The sequence of the entries into each arm was recorded. Spontaneous alternation was calculated as the percentage of the consecutive entry into each arm as triplets to the total number of possible alternations.

In vivo *transcranial imaging and data analysis*

Transcranial two-photon imaging and analysis of spine density and dynamics of apical dendritic tufts were performed as previously described (Zuo et al., 2005a; Xu et al., 2009; Yu and Zuo, 2014). Spines were classified into four categories (mushroom, stubby, thin, and other spines) based on their lengths and head diameters using previously published criteria (Hodges et al., 2017). All images were analyzed using ImageJ. Spine density was calculated by dividing the number of spines by the length of the dendritic segment on which they reside. Percentage of spines eliminated or formed was calculated as the number of spines eliminated or formed over the total spines counted in the images obtained during the first imaging session.

Sensory deprivation

Whisker trimming was performed as previously described (Zuo et al., 2005b). Mystacial vibrissae on one side of the face (contralateral to the imaging area) were cut to skin level daily between the two images sessions (P30–P37). Control mice were handled similarly daily without whisker trimming.

Environmental enrichment

EE protocol was performed and adapted from a previous protocol (Benaroya-Milshtein et al., 2004). For imaging, following the first imaging session, mice were placed in cages (48 × 25 × 18 cm) filled with toys that vary in size, shape, material, texture, and color; these included items such as igloos with saucer type wheels, plastic tunnels, plastic tubing mazes, wooden logs, and metal running wheels for the mice to interact with. Before placement of the toys in the EE cage, toys went through a cage wash and were wiped with 30% ethanol before being patted dry with a paper towel. To create a novel environment for the mice, the toy location and type of toy was changed every day in the morning.

Experimental design and statistics

One-way or two-way ANOVA was used for statistical analysis (unless otherwise stated) using Prism 7. Statistical analyses for spine data were performed using SigmaPlot 11 (RRID:SCR_003210). Total spine densities of WT and CaMKIIα-RARα cKO mice were directly compared using an unpaired two-tailed Student's *t* test. A two-way ANOVA followed by Holm–Sidak *post hoc* pairwise comparisons was used to compare the distribution of spine morphologies of WT and CaMKIIα-RARα cKO mice at P30, and to analyze whether genotype and condition affected dynamics of total spines or different spine types. Statistical significance was defined as $p < 0.05$.

Results

Altered texture preference in mice lacking RARα expression in CaMKIIα-RARα cKO

To examine RARα's function in cortical circuits, we selectively deleted RARα in mature forebrain excitatory neurons by crossing the floxed RARα conditional knock-out (RAR$\alpha^{fl/fl}$) mice (Chapellier et al., 2002; Sarti et al., 2012) with CaMKIIα-Cre driver mice (Tsien et al., 1996). Cre expression in the line of CaMKIIα-Cre we used starts during the third postnatal week (Tonegawa et al., 1996), thus ensuring normal RARα expression during brain development. We further crossed these mice (hereinafter referred to as CaMKIIα-RARα cKO mice) with *thy1*-YFP-H mice (Feng et al., 2000) that express YFP in a subset of L5 PNs, making it possible to monitor dendritic spine dynamics *in vivo* by transcranial two-photon imaging. The number of RARα-expressing neurons in S1 L5 PNs was reduced by ~80% in CaMKIIα-RARα cKO mice compared with wild-type (WT; RAR$\alpha^{fl/fl}$ without Cre allele) littermates at postnatal day 30 (P30), as quantified by single-cell RT-qPCR (Fig. 1*A*). CaMKIIα-RARα cKO mice exhibited normal barrel formation and a normal gross morphology of S1 (Fig. 1*B*).

Rodents distinguish different textures using their whiskers, which relies on normal sensory processing in the S1. Thus, we probed somatosensory processing using a texture preference test. Mice were presented with two textures (i.e., commercial sandpaper with different roughness characterized by differences in grain size), and the percentage of time spent exploring each texture was

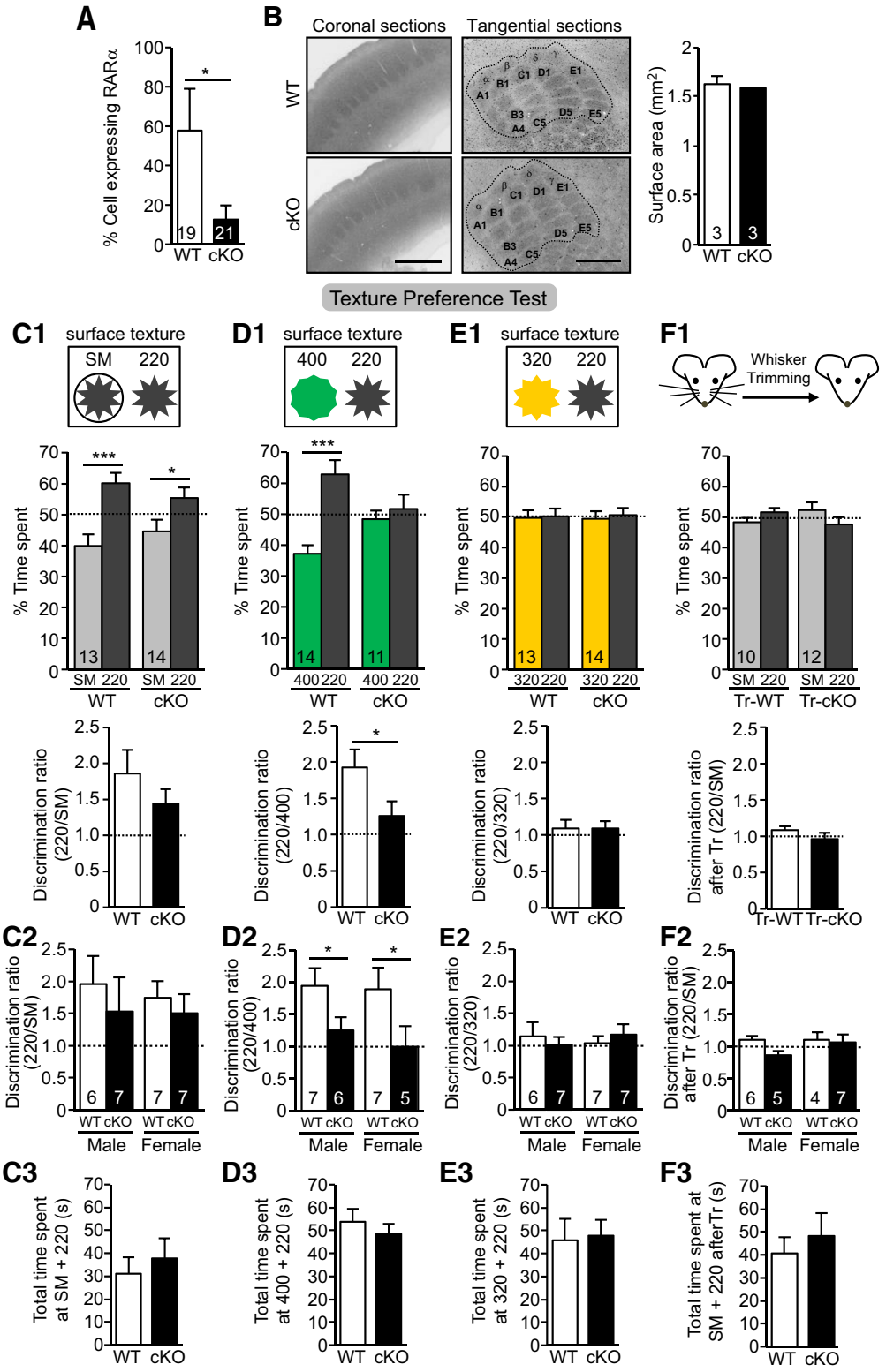

Figure 1. Altered texture preference in P30 CaMKIIα-RARα cKO mice. ***A***, Quantification of percentage of L5 PN expressing RARα mRNA measured by single-cell RT-qPCR of P30 WT and CaMKIIα-RARα cKO mice. *$p < 0.05$, $n =$ the number of cells used from three mice per genotype. ***B***, Representative images of P30 WT and CaMKIIα-RARα cKO S1 cortices visualized by cytochrome *c* staining in coronal and tangential sections. Quantification of S1 surface area outlined in images. Scale bar, 500 μm. ***C1–F1***, Texture discrimination tests with different pairs of surface textures in WT and CaMKIIα-RARα cKO mice. Top diagrams indicate surface texture pairs used for each test. Percentage time spent at each texture (middle; *$p < 0.05$, ***$p < 0.001$) and discrimination ratios (bottom; *$p < 0.05$) of rough texture (220) versus smoother surface (***C1***, SM; ***D1***, 400; ***E1***, 320) are quantified. ***F1***, Quantification of texture discrimination of rough texture (220) versus SM in whisker-trimmed mice (Tr). ***C2–F2***, Comparison of discrimination ratio in male and female WT and CaMKIIα-RARα cKO mice for each test (*$p < 0.05$). ***C3–F3***, Total time spent at textures in each test. In all graphs, data represent mean values ± SEM; $n =$ the number of animals used for each condition. Statistical significance was determined using one-way ANOVA.

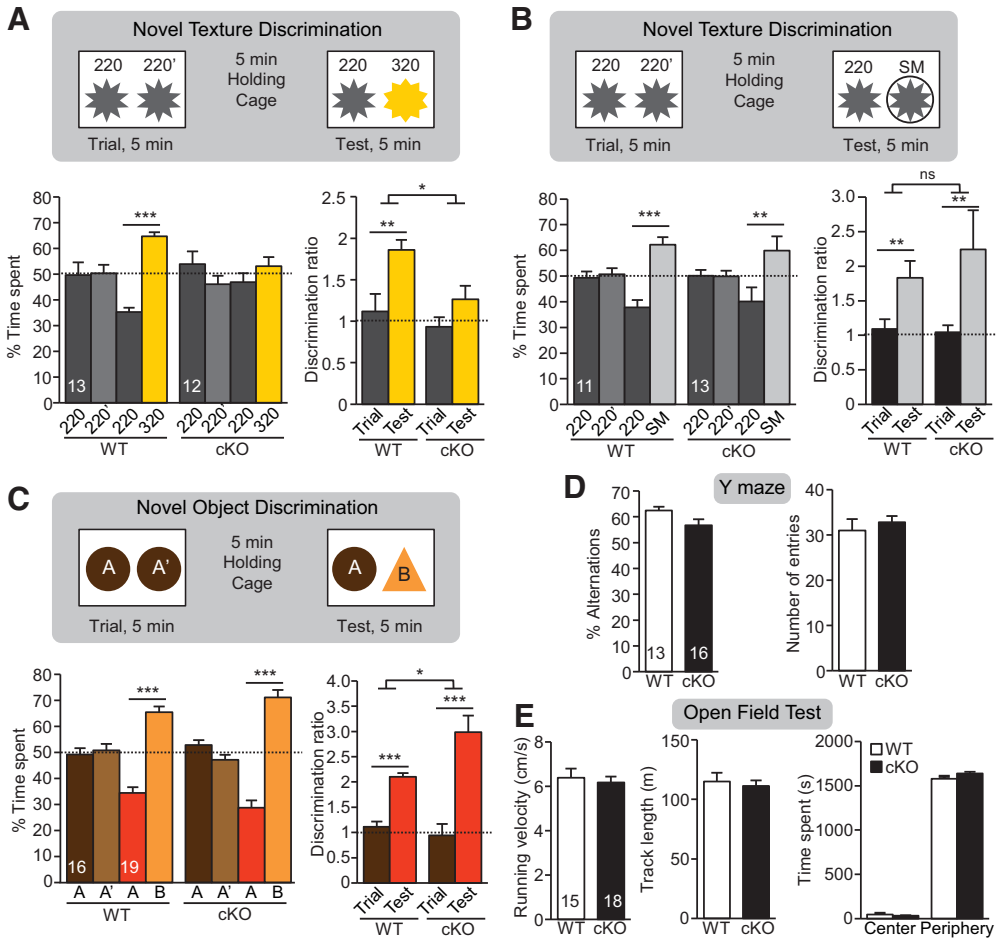

Figure 2. Impaired novel texture discrimination in P30 CaMKIIα-RARα cKO mice. ***A***, ***B***, Schematics (top) and quantification (bottom) of novel texture discrimination between 220/320 pairs (***A***) and 220/SM pairs (***B***). Bar graphs show percentage of time spent at each texture during the trial and test phases (bottom left; $*p < 0.05$, $**p < 0.01$, $***p < 0.001$, one-way ANOVA) and discrimination ratios between the texture pairs during the trial and test phases (bottom right; $**p < 0.01$, $*p < 0.05$, two-way ANOVA). ***C***, Schematics (top) and quantification (bottom) novel object discrimination. Bar graphs show percentage of time spent at each object during the trial and test phase (bottom left; $***p < 0.001$, one-way ANOVA) and discrimination ratios between the two objects during the trial and test phases (bottom right; $*p < 0.05$, $*p < 0.05$, $***p < 0.001$, two-way ANOVA). ***D***, Quantification of Y-maze test. Bar graphs show percentage of alternation (left) and number of total entries (right). ***E***, Quantification of open-field test. Bar graphs show average velocity (left), average track length (middle), and average time spend in the center and periphery of the chamber during open-field test (right). In all graphs, data represent mean values ± SEM; n = the number of animals used for each condition.

measured (Fig. 1*C1–E1*). Four different textures with similar color but increasing roughness were used in this study: SM (220 grit sandpaper wrapped with cellophane), and 400, 320, and 220 grit (note that roughness is inversely correlated to grit number). We found that both WT and CaMKIIα-RARα cKO mice preferred 220 grit sandpaper to SM (Fig. 1*C1*). WT mice also preferred 220 grit sandpaper to 400 grit (less rough) sandpaper, but CaMKIIα-RARα cKO mice did not differentiate between 400 and 220 grit (Fig. 1*D1*). Neither WT nor CaMKIIα-RARα cKO mice showed a preference when offered the choice between 320 and 220 grit paper, which are very similar in roughness (Fig. 1*E1*). Bilateral whisker trimming eliminated the preference between SM and 220 grit in both WT and CaMKIIα-RARα cKO mice (Fig. 1*F1*), confirming that texture detection behavior is whisker-dependent. This behavior was not specific to gender (Fig. 1*C2–F2*) and the total time the mice spent with the different textures were comparable (Fig. 1*C3–F3*).

Deficient texture discrimination in CaMKIIα-RARα cKO mice

In addition to decreased ability for sensory perception, other factors (e.g., motivational and emotional states) could also contribute to the altered texture preference exhibited by CaMKIIα-RARα cKO mice. Thus we further investigated whisker-dependent texture discrimination using a previously established paradigm with slight modifications (Wu et al., 2013). We chose the two textures (220 and 320 grit) for which WT and CaMKIIα-RARα cKO mice showed no baseline preference (Fig. 1*E*). After being presented with two columns with identical textures (220 grit) for 5 min, the mice were put into a holding cage for a 5 min break when both columns were replaced, one with the same texture (familiar, 220 grit) and the other with a finer texture (novel, 320 grit; Fig. 2*A*). The mice were then brought back to the test chamber and allowed to explore freely for another 5 min. Whereas the WT mice preferred the novel texture in the test phase, evidenced by significantly more time spent exploring the novel texture and an increase in the discrimination ratio, the CaMKIIα-RARα cKO mice showed no such preference (Fig. 2*A*), suggesting an impairment in texture discrimination. Importantly, when the novel texture discrimination test was repeated with two textures of greater difference (i.e., SM and 220 grit), both WT and CaMKIIα-RARα cKO mice showed normal discrimination (Fig. 2*B*), indicating that CaMKIIα-RARα cKO mice have normal working memory as well as motivation for exploration, and that the impaired novel

texture discrimination observed with the 220 and 320 grit surfaces is likely due to their inability to tell the two similar textures apart.

To further test the possibility that impaired short-term working memory is responsible for the lack of texture discrimination in the CaMKIIα-RARα cKO mice, we subjected the mice to the novel object recognition test (NOR; using Lego pieces with different shapes and colors), and to the spontaneous Y-maze test. As mice typically prefer exploring a novel object over a familiar one (in the NOR test) and exploring a new arm instead of returning to the arm previously entered (in Y maze), these behavioral tasks evaluate working memory and motivation for exploration. Both WT and CaMKIIα-RARα cKO mice preferred the novel object during the test phase of the NOR test (Fig. 2*C*), and showed comparable percentages of alternations and number of entries in the spontaneous Y-maze test (Fig. 2*D*), indicating that short-term working memory is intact and exploration behavior is normal in the CaMKIIα-RARα cKO mice. Additionally, WT and CaMKIIα-RARα cKO mice showed similar locomotive and anxiety levels as indicated by comparable running velocity, average track length, and time spent in the center of the chamber in the open-field test (Fig. 2*E*). Together, these data establish that selective deletion of RARα in mature forebrain excitatory neurons causes impaired information processing in the somatosensory cortical circuits.

Region-specific deletion of RARα in somatosensory cortices or L5 PNs impairs texture discrimination

Because the CaMKIIα-Cre driver line targets excitatory neurons throughout the forebrain, it is unclear whether the diminished texture discrimination in the CaMKIIα-RARα cKO mice is due to the loss of RARα within S1. To delete RARα selectively in S1, we bilaterally injected AAVs encoding Cre recombinase fused with GFP (GFP-Cre) under control of the synapsin promoter (Kaeser et al., 2011) into S1 of $RAR\alpha^{fl/fl}$ mice at P0 (hereinafter referred to as S1-RARα cKOs; Fig. 3*C*). Injection of AAVs encoding inactive mutant GFP-Cre (mCre) was used as a control. Reduction of RARα expression by GFP-Cre expression was confirmed with single-cell qRT-PCT (Fig. 3*A*). The barrel formation was unaffected by viral injection and acute deletion of RARα through viral expression of Cre (Fig. 3*B*). When tested at P30, control mice preferred the rougher surface between 400 and 220 grit, whereas S1-RARα cKO mice showed no preference (Fig. 3*D*). As an additional control, $RAR\alpha^{fl/fl}$ mice receiving bilateral injections of mCre- or Cre-expressing AAVs into V1 were subjected to the same test, and were found to behave similarly to WT mice (Fig. 3*F*,*G*). Both S1-RARα cKO and V1-RARα cKO mice performed normally in the Y-maze test (Fig. 3*E*,*H*). Moreover, texture discrimination test in S1-RARα cKO mice revealed an impaired ability to discriminate textures of smaller differences in roughness (220 vs 320 grit; Fig. 3*I*) but not textures of greater differences (220 vs SM; Fig. 3*J*), which is consistent with our findings in the CaMKIIα-RARα cKO mice (Fig. 2*A*,*B*). Thus, RARα-dependent synaptic RA signaling is specifically required in S1 cortex for normal sensory discrimination.

L5 PNs constitute one of the major outputs of the sensory cortex (Veinante et al., 2000; Aronoff et al., 2010; Feldmeyer, 2012; Harris and Shepherd, 2015), leading us to ask whether RARα expression in L5 PNs is required for normal texture preference. We crossed the L5-specific Cre-driver line Rbp4-Cre (DeNardo et al., 2015) with the $RAR\alpha^{fl/fl}$ mouse (hereinafter referred to as L5 PN-RARα cKO mouse) and confirmed reduction in RARα mRNA levels (Fig. 4*A*). Again, these mice had normal barrel formation (Fig. 4*B*) and normal Y-maze performance (Fig. 4*D*) but lacked texture preference (Fig. 4*C*), similar to what we observed in the CaMKIIα-RARα cKO (Fig. 1*D*) and S1-RARα cKO mice (Fig. 3*D*). Together, these data indicate that postnatal RARα expression in L5 PNs of S1 is needed for normal texture preference.

It is worth pointing out that unlike the CaMKII-RARα line, where Cre expression starts at ~P19 in the cortex and hippocampus (Tsien et al., 1996), Cre expression in the P0 S1-injected and Rbp4-RARα lines is turned on much earlier (i.e., perinatally; Grant et al., 2016). Thus, there may be unexpected developmental effects due to early deletion of RARα in S1 neurons or L5 PNs. The normal gross morphology of the barrel cortex and similar behavioral outcomes from mice with the three different genetic manipulations, however, argues that either the developmental effect of early postnatal deletion of RARα is minimal, or that the developmental effect of RARα deletion does not contribute to the performance of the behavior tests chosen for this study.

RARα plays a role in experience-dependent spine elimination

We next asked what mechanism may underlie the impairment in sensory discrimination induced by loss of synaptic RA signaling in S1 pyramidal neurons. Changes in synaptic connectivity through formation and elimination of dendritic spines correlate with functional changes in the brain (Kasai et al., 2010; Hayashi-Takagi et al., 2015). Recent work showed that spine loss and atrophy of S1 L5 PN apical dendrites correlated with defects in texture discrimination in mice (Chen et al., 2017). Thus, we investigated whether structural dynamics of dendritic spines are altered in the CaMKIIα-RARα cKO mice. Using *in vivo* two-photon imaging, we followed the same apical dendritic branches of YFP+ L5 PNs in the superficial layer of S1 over 7 d (Fig. 5*A*). We found that CaMKIIα-RARα cKO mice had normal spine density (Fig. 5*B*) and distribution of different spine types (i.e., spines with different morphology; Fig. 5*C*) at P30. However, a closer examination revealed a small but significant increase in spines elimination over 7 d in CaMKIIα-RARα cKOs compared with WT littermates (Fig. 5*D*,*E*). By contrast, spine formation was comparable (Fig. 5*G*). As experience-dependent postnatal spine elimination is important for the refinement of neuronal circuits (Zuo et al., 2005b), we next asked whether elevated spine elimination in CaMKIIα-RARα cKO mice requires sensory inputs. To do so, we trimmed the whiskers unilaterally and imaged the contralateral S1. Consistent with previous studies (Zuo et al., 2005b; Yu et al., 2013), we found that whisker trimming significantly reduced spine elimination, but not formation, in WT and even more so in CaMKIIα-RARα cKO mice (Fig. 5*E*,*G*). As a result, whisker-trimmed WT and whisker-trimmed CaMKIIα-RARα cKO mice exhibited similar spine dynamics (Fig. 5*E*,*G*), suggesting that sensory inputs are required for the elevated spine elimination observed in CaMKIIα-RARα cKO mice.

As the morphology of dendritic spines correlate with their function and stability (Harris and Stevens, 1989; Schikorski and Stevens, 1999; Matsuzaki et al., 2001; Kasai et al., 2003), we analyzed the dynamics of imaged spines according to their morphological types (i.e., mushroom, thin, stubby and others). We found that thin spines were significantly more likely to disappear over 7 d than other types of spines in WT mice (Fig. 5*F*), consistent with the earlier finding that thin spines have a higher turnover rate and thus are more transient (Holtmaat et al., 2005; Bourne and Harris, 2007). The CaMKIIα-RARα cKO mice showed a comparable level of thin spine elimination to the WT mice (Fig. 5*F*). However, a significantly higher percentage of mushroom

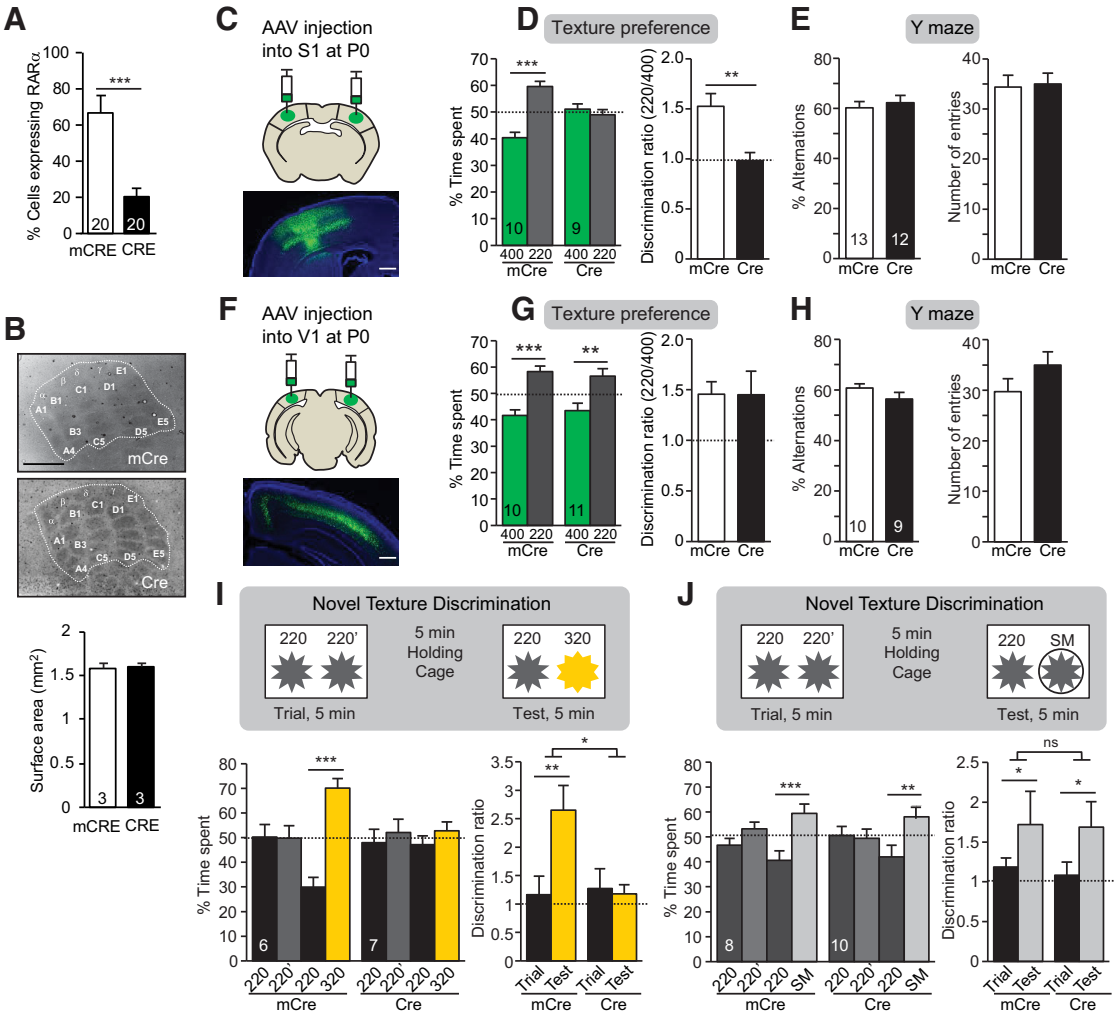

Figure 3. Specific role of RARα in barrel cortex in texture preference and novel texture discrimination. ***A***, Quantification of percentage of L5 PN expressing RARα mRNA measured by single-cell RT-qPCR of P30 WT and S1-RARα cKO mice (***$p < 0.001$, one-way ANOVA; n = the number of cells used from 3 mice per genotype). ***B***, Representative images of P30 WT (mCRE) and S1-RARα cKO (CRE) cortices visualized by cytochrome *c* staining in tangential sections and quantification of S1 surface area outlined in images. Scale bar, 500 μm. ***C***, Representative image of stereotaxic injection into S1 of RARα$^{fl/fl}$ mice of AAV virus expressing synapsin promoter driven active Cre or inactive mCRE. Scale bar, 500 μm. ***D***, Quantification of texture preference in S1-RARα cKO mice. Bar graphs show percentage of time spent at texture 400 and 220 (left; ***$p < 0.001$, one-way ANOVA) and discrimination ratios of the two textures of S1-RARα cKO mice (right; **$p < 0.01$, one-way ANOVA). ***E***, Quantification of Y-maze test in S1-RARα cKO mice. Bar graphs show quantification of percentage of alternation (left) and number of entries (right). ***F***, Representative image of stereotaxic Cre or mCre injection into V1 of RARα$^{fl/fl}$ mice. Scale bar, 500 μm. ***G***, Quantification of texture preference in V1-RARα cKO mice. Bar graphs show percentage of time spent at texture 400 and 220 (left; **$p < 0.01$, ***$p < 0.001$, one-way ANOVA) and discrimination ratios of the two textures of V1-RARα cKO mice (right). ***H***, Quantification of Y-maze test in V1-RARα cKO mice. Bar graphs show quantification of percentage of alternation (left) and number of entries (right). ***I***, ***J***, Schematics (top) and quantification (bottom) of novel texture discrimination in S1-RARα cKO mice with two different texture pairs. Bar graphs show percentage of time spent at each texture during the trial and test phase (bottom left; **$p < 0.01$, ***$p < 0.001$, one-way ANOVA) and discrimination ratios between the two textures during the corresponding phase (right; *$p < 0.05$, **$p < 0.01$, two-way ANOVA). In all graphs, data represent mean values ± SEM, and n represents the number of animals used for each condition unless otherwise stated.

and stubby spines were eliminated in the CaMKIIα-RARα cKO mice compared with WT mice (Fig. 5*F*). By contrast, formation of all spine types was similar between WT and CaMKIIα-RARα cKO mice (Fig. 5*H*). As mushroom spines are believed to be more functionally mature and stable (Harris et al., 1992; Bourne and Harris, 2007), our data suggest that disrupting RA signaling selectively affects the maintenance of stable, mature spines.

We next asked whether sensory deprivation also affects different types of spines differentially. In WT mice, unilateral whisker trimming significantly reduced the elimination of thin spines, but not of other spine types (Fig. 5*F*). In CaMKIIα-RARα cKO mice, by contrast, whisker trimming did not affect thin spine elimination, but decreased the elimination of mushroom and stubby spines to the same level as in whisker-trimmed WT mice (Fig. 5*F*). Moreover, we found that whisker trimming did not significantly alter the formation of any spine types in WT or CaMKIIα-RARα cKO mice (Fig. 5*H*). Together, these data suggest that RARα involvement in experience-dependent spine remodeling depends on the spine type.

Enriched environment improves sensory discrimination and alters spine dynamics in CaMKIIα-RARα cKO mice

An EE provides rich sensory and motor stimulation, promotes neurogenesis and synaptic plasticity in various brain regions, and improves cognitive performance in many behavioral tasks (Eckert and Abraham, 2013). In a final set of experiments, we sought to determine how an EE affects RA-dependent sensory processing. We performed the novel texture discrimination tests after 7 d of EE, using two similar textures (220 vs 320 grit). The WT animals did not have any obvious improvement in their discrim-

ination index after this short-term EE paradigm (compared with the performance of WT animals in Fig. 2*A*, although one must note that the experiments were performed in different cohorts of animals). Moreover, we found that CaMKIIα-RARα cKO mice after EE performed similarly to WT controls regardless of the identity of the familiar and novel texture (Fig. 6*A*,*B*), indicating improved sensory discrimination ability in RARα cKO mice after EE experiences.

Might the effect of EE on texture discrimination be explained in terms of spine dynamics in the CaMKIIα-RARα cKO mice? We first imaged spines at P30, then subjected the mice to EE, and reimaged the same spines 7 d later (Fig. 7*A*). Consistent with previous findings, EE increased both spine formation and elimination in WT mice (Fig. 7*B*,*D*; Yang et al., 2009; Fu et al., 2012; Yu et al., 2013). Interestingly, EE decreased spine elimination without changing spine formation in CaMKIIα-RARα cKO mice, rendering the spine dynamics comparable with that of WT mice raised in standard cages (Fig. 7*B*,*D*). Further analysis revealed that EE significantly increased the elimination of mushroom and stubby spines in the WT mice, but paradoxically reduced the elimination of stubby spines in the CaMKIIα-RARα cKO mice (Fig. 7*C*). Additionally, EE increased mushroom spine formation in WT mice, but not in CaMKIIα-RARα cKO mice (Fig. 7*E*). Together, EE affects spine dynamics of CaMKIIα-RARα cKO and WT mice in different ways: CaMKIIα-RARα cKO mice housed under EE condition exhibit comparable spine dynamics to WT mice housed in standard cages.

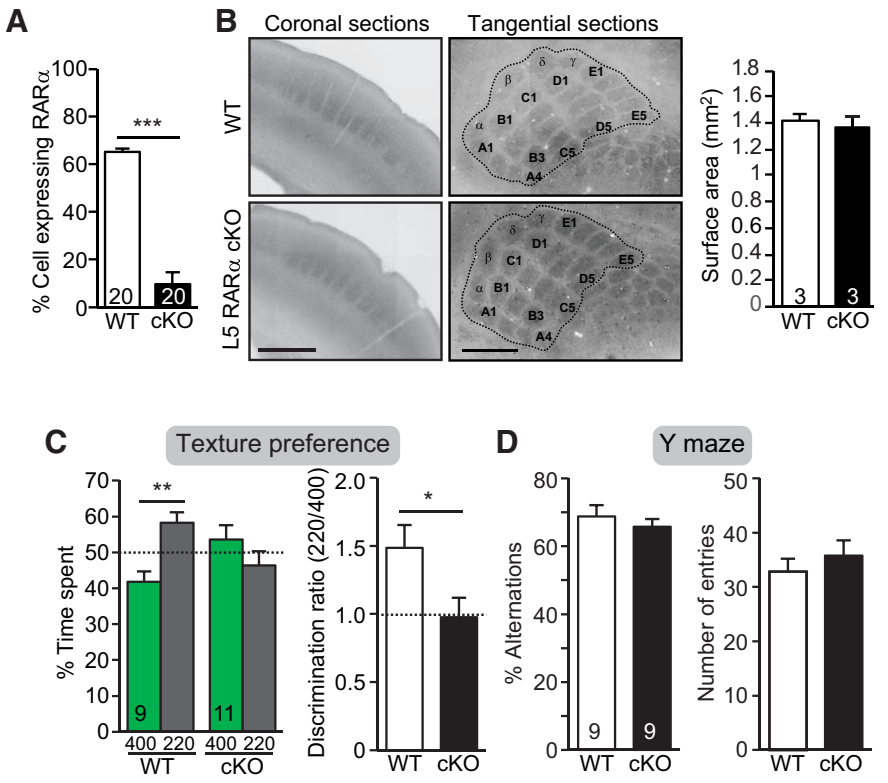

Figure 4. Deletion of RARα expression in L5 PNs altered texture preference. ***A***, Quantification of percentage of L5 PN expressing RARα mRNA measured by single-cell RT-qPCR of P30 WT and L5-RARα cKO mice (***$p < 0.001$; $n =$ the number of cells used from 3 mice per genotype). ***B***, Representative images of intact barrel formation of L5 PN-RARα cKO mice in coronal and tangential sections and quantification of S1 surface area outlined in images. Scale bar, 500 μm. ***C***, Quantification of texture preference in L5 PN-RARα cKO mice. Bar graphs show percentage of time spent at texture 400 and 220 (left; **$p < 0.01$) and discrimination ratios of the two textures (right; *$p < 0.05$). ***D***, Quantification of Y-maze performance in L5 PN-RARα cKO mice. Bar graphs show percentage of alternation (left) and quantification of number of entries (right). In all graphs, data represent average mean ± SEM; *n* indicates the numbers of mice analyzed. Statistical significance was determined using one-way ANOVA.

Discussion

The importance of RA signaling in synaptic function and plasticity has been well established *in vitro* (Chen et al., 2014b; Arendt et al., 2015a). Here, we tested the *in vivo* significance of synaptic RA signaling by examining the impact of postnatal RARα deletion on sensory information processing and dendritic spine dynamics in pyramidal neurons of the somatosensory cortex. We observed behavioral deficits in texture discrimination with three different RARα deletion strategies: deletion of RARα in all forebrain excitatory neurons with a CaMKIIα-Cre driver line, deletion of RARα in cortical S1 neurons with AAV-Cre injection, and deletion of RARα in L5 PNs with Rbp4-Cre driver line. The normal locomotion and short-term working memory in these mice indicate that the texture discrimination deficit represents a specific impairment caused by an important, but subtle impairment in cortical circuit function in S1. More specifically, synaptic dysfunction in S1 L5 PNs, in which RARα expression is reduced by 80% (Fig. 1*A*), is likely the main contributor to the observed phenotype because it is the only neuronal population affected by all three genetic manipulations. This notion is further supported by our *in vivo* imaging data examining spine dynamics on the apical dendrites of L5 PNs. Defects in mushroom spine elimination in the CaMKIIα-RARα cKO suggests that RARα signaling may be involved in mature spine maintenance in L5 PNs. Following whisker trimming, CaMKIIα-RARα cKO and WT mice show comparable spine dynamics of all spine categories, suggesting that the impact of RARα on spine elimination is activity-dependent (i.e., in the absence of sensory input, spine maintenance does not require RARα function). Introduction of an EE experience to the CaMKIIα-RARα cKO mice rescued the texture discrimination phenotype and partially restored spine dynamics back to those of WT with standard cage experience, suggesting that both RARα-dependent and RARα-independent plasticity processes are at play in parallel to support cortical circuit functions. Together, our data demonstrate that normal cortical circuit-dependent sensory information processing and experience-driven spine remodeling in S1 require normal RARα function.

How does impaired RA signaling through RARα deletion contribute to impaired texture discrimination? Whisker movement across textures generates complex whisker micromotions, from which information is extracted and processed in S1 (Jadhav et al., 2009). Three main theories have been proposed to explain how textures are encoded in S1: the mean speed theory, the slip-stick theory and the differential resonance theory (Jadhav and Feldman, 2010). It is generally believed that texture information is encoded by L2/3 neurons (Garion et al., 2014), but it remains unknown how this texture information is integrated into and processed within L5 PNs whose activity eventually guides the behavioral output. Despite the largely unexplored mechanism of whisker-dependent texture encoding, it is conceivable that RARα

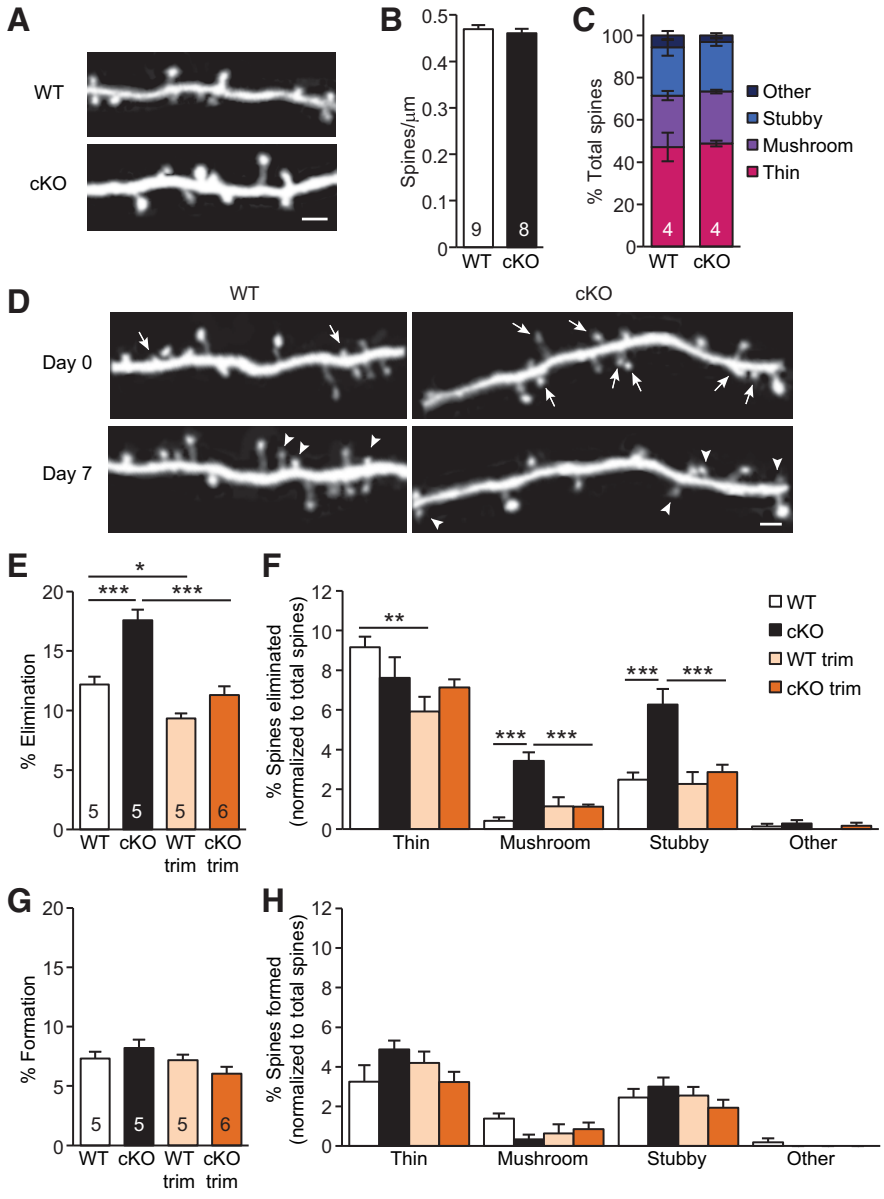

Figure 5. Experience-dependent elimination of spines is elevated in L5 PNs of P30 CaMKIIα-RARα cKO mice. ***A***, Representative images taken by *in vivo* transcranial imaging of YFP in WT and CaMKIIα-RARα cKO mice. Scale bar, 2 μm. ***B***, Quantification of spine density in P30 WT and CaMKIIα-RARα cKO mice (7–12 dendrites per animal were analyzed, Student's *t* test). ***C***, Distribution of spine types in WT and CaMKIIα-RARα cKO mice (two-way ANOVA). ***D***, Repeated imaging of the same dendritic branches over a 7 d interval in the barrel cortex of WT and cKO mice under control conditions reveal newly formed spines (arrowheads), and eliminated spines (arrows). Scale bar, 2 μm. ***E***, Quantification of the percentages of spines eliminated over 7 d in the barrel cortex of WT and cKO mice under control and trimmed conditions (Trim; $^{*}p < 0.05$, $^{***}p < 0.001$, two-way ANOVA). ***F***, Quantification of the percentages of eliminated spine types normalized to total spines eliminated ($^{**}p < 0.01$, $^{***}p < 0.001$, two-way ANOVA). ***G***, Quantification of the percentages of spines formed over 7 d in the barrel cortex of WT and cKO mice under control and whisker-trimmed conditions (two-way ANOVA). ***H***, Quantification of the percentages of formed spine types normalized to total spines formed (two-way ANOVA). In all graphs, data represent average mean ± SEM; *n* indicates the numbers of mice analyzed.

deletion in L5 PNs impairs experience-dependent homeostatic synaptic plasticity that fine-tunes the strength of active synapses (i.e., a balance maintained through elimination of immature thin spines and maintenance of mature mushroom-type spines), and subsequently affects L5 PNs' ability to integrate sensory input from L2/3 neurons and to generate appropriate behavioral output. It is worth noting that different mechanisms may be used to encode texture differences that are large or finer (Diamond et al., 2008; Jadhav et al., 2009). In our hands, RARα deletion only affects discrimination of texture differences that are finer but not large, thus synaptic RA signaling likely contributes to fine texture discrimination.

RA signaling is thought to be essential for synaptic plasticity and memory formation in adult brain (Chiang et al., 1998; Cocco et al., 2002), thus it may be surprising that in the CaMKIIα-RARα KO and Rbp4-RARα KO mice, where RARα deletion is not confined to S1, no memory deficit was observed. Previous studies have focused on hippocampal synaptic plasticity and hippocampus-dependent memory tasks. In our hands, we also found altered hippocampal synaptic plasticity and hippocampus-dependent long-term memory deficit in RARα-deficient mice (unpublished observation). The working memory assays used in this study (Y maze and novel object recognition) use short retention time, which was designed specifically to allow direct comparison with and control for the texture discrimination tasks used to probe S1 sensory processing. Working memory tests with short retention intervals do not require hippocampal function (Smith et al., 2014), thus our results of normal working memory do not contradict previous reports on hippocampal memory deficits, neither do they indicate that there is no deficit in long-term memory related to other sensory modalities.

To gain a mechanistic understanding of the sensory discrimination deficit in the RARα-deficient mice, we probed spine dynamics on the apical dendrites of S1 L5 PNs. Morphological classifications of spines showed that the RARα deletion led to a selective increase in the elimination of mushroom and stubby spines, with no obvious effect on thin spines. This observation may be explained by several possible hypotheses: (1) RARα deletion causes mushroom-type spines to be transformed into thin-type spines. This would predict that thin-type spines occupy a higher proportion of the total spines in neurons with RARα deletion, which is not consistent with our observation (Fig. 5*C*). (2) RARα deletion leads to an aberrant decrease in the survival/maintenance of mushroom spines. In general, mushroom-shaped spines are thought to be more functionally mature and remain stable for a longer period compared with thin spines (Harris et al., 1992; Holtmaat et al., 2005; Bourne and Harris, 2007). The fact that RARα deletion specifically targets this population of spines suggests that RARα functions at spines that are normally mature and active. This may explain why the spine elimination phenotype is rescued in whisker-trimmed mice because the lack of sensory input eliminates/reduces the activity differences between strong (mushroom) and weak (thin) spines. The function of synaptic RA signaling was initially discovered in the context of homeostatic plasticity (Maghsoodi et al., 2008), and RARα is thought to be a

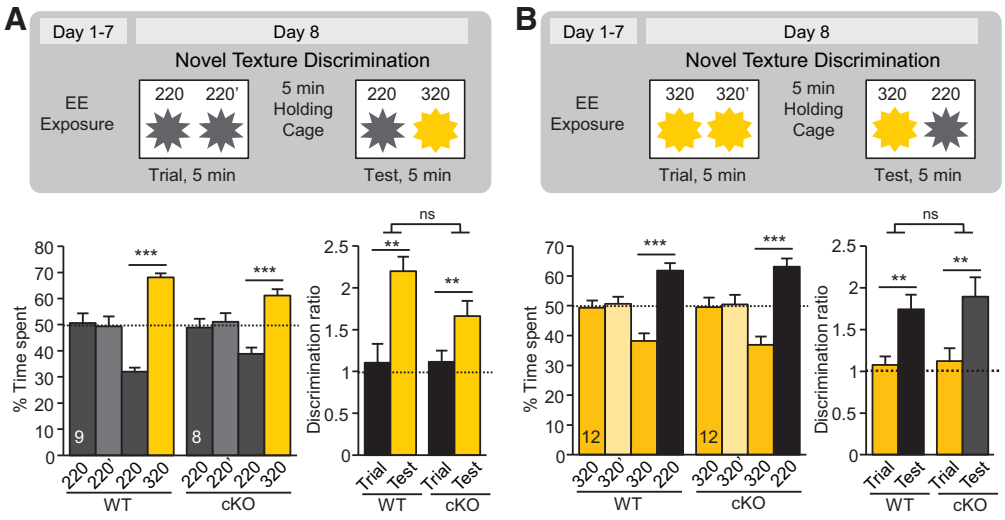

Figure 6. Effects of enriched environment on novel texture discrimination in CaMKIIα-RARα cKO mice. ***A***, ***B*** Schematics (top) and quantification (bottom) of novel texture discrimination between 220/320 pairs (***A***) and 320/220 pairs (***B***). Bar graphs show percentage of time spent at each texture during the trial and test phases (bottom left; $^{***}p < 0.001$, one-way ANOVA) and discrimination ratios between the texture pairs during the trial and test phases (bottom right; $^{**}p < 0.01$, two-way ANOVA). In all graphs, data represent mean values ± SEM; *n* indicates the numbers of mice analyzed.

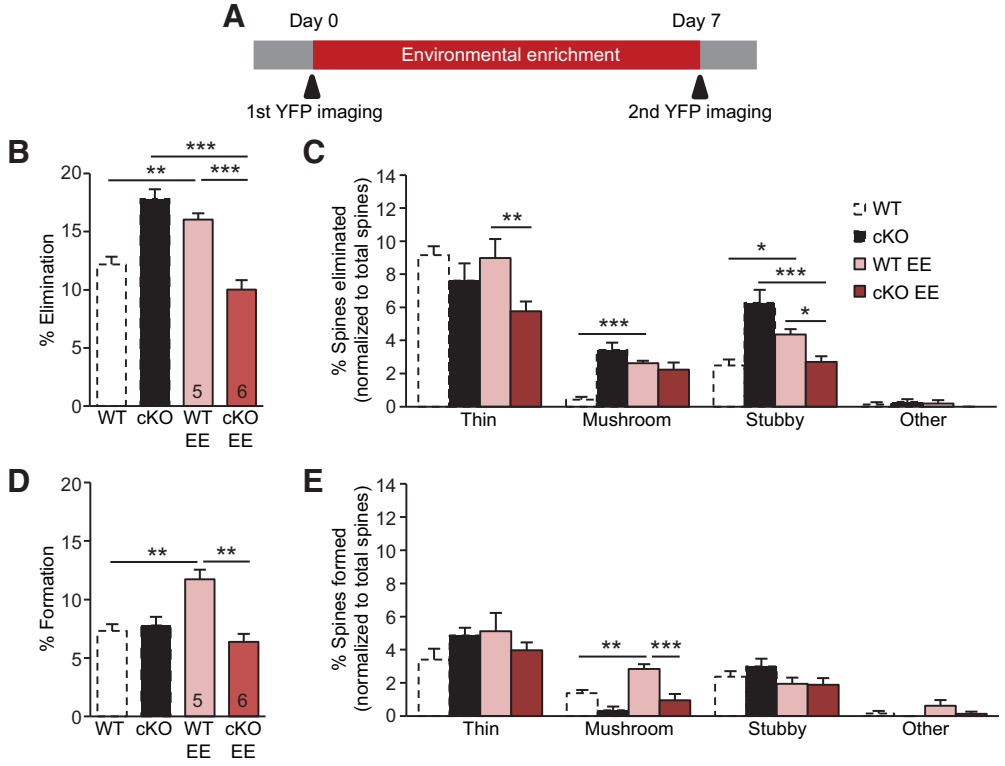

Figure 7. Effects of enriched environment on spine dynamics in CaMKIIα-RARα cKO mice. ***A***, Diagram of EE and *in vivo* spine imaging protocol. ***B***, Quantification of the percentages of spines eliminated over 7 d in the barrel cortex of WT and CaMKIIα-RARα cKO mice under control and EE conditions ($^{**}p < 0.01$, $^{***}p < 0.001$, two-way ANOVA). ***C***, Quantification of the percentages of eliminated spine types normalized to total spines eliminated ($^{*}p < 0.05$, $^{**}p < 0.01$, $^{***}p < 0.001$, two-way ANOVA). ***D***, Quantification of the percentages of spines formed over 7 d in the barrel cortex of WT and CaMKIIα-RARα cKO mice under control and EE conditions ($^{**}p < 0.01$, two-way ANOVA). ***E***, Quantification of the percentages of formed spine types normalized to total spines formed ($^{**}p < 0.01$, $^{***}p < 0.001$, two-way ANOVA). In all graphs, data represent mean values ± SEM; *n* indicates the numbers of mice analyzed.

translational suppressor that inhibits dendritic protein synthesis under normal synaptic transmission and elevated dendritic calcium levels (Poon and Chen, 2008; Wang et al., 2011). Thus, it is reasonable to speculate that deletion of RARα will have a significant impact on the function of active synapses, which are formed usually on mature spines.

It remains to be understood how EE impacts sensory discrimination and spine dynamics in RARα deletion mice. Given how sensory deprivation through whisker trimming reverses the excessive spine elimination observed in RARα-deficient mice raised in standard cage conditions, it is counterintuitive that EE improves sensory discrimination: why does not EE further impair

sensory discrimination and exacerbate abnormal spine dynamics? A key conceptual realization here is that EE is not simply a behavioral experience opposite to whisker trimming. In other words, compared with total sensory deprivation, EE does not merely increase sensory input and cortical circuit activation, but enhances behaviorally meaningful sensory input and provides structured activation of cortical circuits. Previous reports show that EE enhances learning and social interactions and improves cognitive performance (Nithianantharajah and Hannan, 2006). Distinct from artificial stimulation paradigms that induce a single type of plasticity at a particular set of synapses (e.g., theta burst or tetanus stimulation in CA1 synapses induces LTP), EE provides a wide spectrum of natural stimuli to synapses in many neural circuits involved in sensory processing, motor generation, memory formation and other cognitive and emotional functions. Thus, it is conceivable that multiple forms of synaptic plasticity are induced by EE, including Hebbian and non-Hebbian plasticity; and that these synaptic changes rewire neural circuits to enable the mouse to better adapt to its environment. Our previous work showed that synaptic RA signaling is specific for homeostatic synaptic plasticity, and is not directly involved in Hebbian plasticity (i.e., normal LTP in RARα KO neurons; Arendt et al., 2015a). Thus, enhanced sensory experience by EE may invoke intense Hebbian plasticity within and outside of S1 despite abnormal homeostatic synaptic plasticity, all of which could contribute to differences of EE-induced spine dynamics between WT and RARα-deficient mice and restoration of sensory discrimination in the RARα-deficient mice.

Acting through a molecular mechanism distinct from its well known genomic regulation (Chambon, 1996), RA rapidly changes excitatory and inhibitory synaptic strength under the influence of activity (Maghsoodi et al., 2008; Sarti et al., 2013), thus impacting Hebbian plasticity through an altered synaptic excitation/inhibition balance (Arendt et al., 2015a; Yee et al., 2017). Indeed, vitamin A deficiency (which depletes RA) impairs hippocampal Hebbian plasticity and learning (Chiang et al., 1998; Misner et al., 2001; Cocco et al., 2002). Moreover, a study using a dominant-negative form of RARα expressed in the adult forebrain demonstrated impairments in AMPAR-mediated synaptic transmission, hippocampal LTP, hippocampal-dependent social recognition, and spatial memory (Nomoto et al., 2012). Our study took advantage of the rich array of mouse genetic tools to dissect the function of RARα in sensory discrimination in an *in vivo* setting, and provides hopefully compelling evidence for a role of synaptic RA signaling in experience-dependent spine dynamics and cortical circuit function. Much additional work is necessary to elucidate how regulation of synaptic and spine function is achieved through synaptic RA signaling, and how altered RA signaling leads to aberrant circuit activity that gives rise to altered behavioral output.

References

Arendt KL, Zhang Y, Jurado S, Malenka RC, Südhof TC, Chen L (2015a) Retinoic acid and LTP recruit postsynaptic AMPA receptors using distinct SNARE-dependent mechanisms. Neuron 86:442–456. CrossRef Medline

Arendt KL, Zhang Z, Ganesan S, Hintze M, Shin MM, Tang Y, Cho A, Graef IA, Chen L (2015b) Calcineurin mediates homeostatic synaptic plasticity by regulating retinoic acid synthesis. Proc Natl Acad Sci U S A 112:E5744–5752. CrossRef Medline

Aronoff R, Matyas F, Mateo C, Ciron C, Schneider B, Petersen CC (2010) Long-range connectivity of mouse primary somatosensory barrel cortex. Eur J Neurosci 31:2221–2233. CrossRef Medline

Benaroya-Milshtein N, Hollander N, Apter A, Kukulansky T, Raz N, Wilf A, Yaniv I, Pick CG (2004) Environmental enrichment in mice decreases anxiety, attenuates stress responses and enhances natural killer cell activity. Eur J Neurosci 20:1341–1347. CrossRef Medline

Bourne J, Harris KM (2007) Do thin spines learn to be mushroom spines that remember? Curr Opin Neurobiol 17:381–386. CrossRef Medline

Chambon P (1996) A decade of molecular biology of retinoic acid receptors. FASEB J 10:940–954. CrossRef Medline

Chapellier B, Mark M, Garnier JM, LeMeur M, Chambon P, Ghyselinck NB (2002) A conditional floxed (*loxP*-flanked) allele for the retinoic acid receptor alpha (RARα) gene. Genesis 32:87–90. CrossRef Medline

Chen JL, Nedivi E (2013) Highly specific structural plasticity of inhibitory circuits in the adult neocortex. Neuroscientist 19:384–393. CrossRef Medline

Chen CC, Lu J, Zuo Y (2014a) Spatiotemporal dynamics of dendritic spines in the living brain. Front Neuroanat 8:28. CrossRef Medline

Chen L, Lau AG, Sarti F (2014b) Synaptic retinoic acid signaling and homeostatic synaptic plasticity. Neuropharmacology 78:3–12. CrossRef Medline

Chen CC, Bajnath A, Brumberg JC (2015) The impact of development and sensory deprivation on dendritic protrusions in the mouse barrel cortex. Cereb Cortex 25:1638–1653. CrossRef Medline

Chen CC, Lu J, Yang R, Ding JB, Zuo Y (2017) Selective activation of parvalbumin interneurons prevents stress-induced synapse loss and perceptual defects. Mol Psychiatry. Advance online publication. CrossRef Medline

Chiang MY, Misner D, Kempermann G, Schikorski T, Giguère V, Sucov HM, Gage FH, Stevens CF, Evans RM (1998) An essential role for retinoid receptors RARbeta and RXRgamma in long-term potentiation and depression. Neuron 21:1353–1361. CrossRef Medline

Cocco S, Diaz G, Stancampiano R, Diana A, Carta M, Curreli R, Sarais L, Fadda F (2002) Vitamin A deficiency produces spatial learning and memory impairment in rats. Neuroscience 115:475–482. CrossRef Medline

Colgan LA, Yasuda R (2014) Plasticity of dendritic spines: subcompartmentalization of signaling. Annu Rev Physiol 76:365–385. CrossRef Medline

DeNardo LA, Berns DS, DeLoach K, Luo L (2015) Connectivity of mouse somatosensory and prefrontal cortex examined with trans-synaptic tracing. Nat Neurosci 18:1687–1697. CrossRef Medline

Diamond ME, von Heimendahl M, Arabzadeh E (2008) Whisker-mediated texture discrimination. PLoS Biol 6:e220. CrossRef Medline

Eckert MJ, Abraham WC (2013) Effects of environmental enrichment exposure on synaptic transmission and plasticity in the hippocampus. Curr Top Behav Neurosci 15:165–187. CrossRef Medline

Feldmeyer D (2012) Excitatory neuronal connectivity in the barrel cortex. Front Neuroanat 6:24. CrossRef Medline

Feng G, Mellor RH, Bernstein M, Keller-Peck C, Nguyen QT, Wallace M, Nerbonne JM, Lichtman JW, Sanes JR (2000) Imaging neuronal subsets in transgenic mice expressing multiple spectral variants of GFP. Neuron 28:41–51. CrossRef Medline

Földy C, Darmanis S, Aoto J, Malenka RC, Quake SR, Südhof TC (2016) Single-cell RNAseq reveals cell adhesion molecule profiles in electrophysiologically defined neurons. Proc Natl Acad Sci U S A 113:E5222–5231. CrossRef Medline

Fu M, Zuo Y (2011) Experience-dependent structural plasticity in the cortex. Trends Neurosci 34:177–187. CrossRef Medline

Fu M, Yu X, Lu J, Zuo Y (2012) Repetitive motor learning induces coordinated formation of clustered dendritic spines *in vivo*. Nature 483:92–95. CrossRef Medline

Garion L, Dubin U, Rubin Y, Khateb M, Schiller Y, Azouz R, Schiller J (2014) Texture coarseness responsive neurons and their mapping in layer 2–3 of the rat barrel cortex *in vivo*. eLife 3:e03405. CrossRef Medline

Gerfen CR, Paletzki R, Heintz N (2013) GENSAT BAC cre-recombinase driver lines to study the functional organization of cerebral cortical and basal ganglia circuits. Neuron 80:1368–1383. CrossRef Medline

Grant E, Hoerder-Suabedissen A, Molnár Z (2016) The regulation of corticofugal fiber targeting by retinal inputs. Cereb Cortex 26:1336–1348. CrossRef Medline

Gray EG (1959) Electron microscopy of synaptic contacts on dendrite spines of the cerebral cortex. Nature 183:1592–1593. CrossRef Medline

Harris KD, Shepherd GM (2015) The neocortical circuit: themes and variations. Nat Neurosci 18:170–181. CrossRef Medline

Harris KM, Stevens JK (1989) Dendritic spines of CA 1 pyramidal cells in the rat hippocampus: serial electron microscopy with reference to their biophysical characteristics. J Neurosci 9:2982–2997. CrossRef Medline

Harris KM, Jensen FE, Tsao B (1992) Three-dimensional structure of dendritic spines and synapses in rat hippocampus (CA1) at postnatal day 15

and adult ages: implications for the maturation of synaptic physiology and long-term potentiation. J Neurosci 12:2685–2705. CrossRef Medline

Hayashi-Takagi A, Yagishita S, Nakamura M, Shirai F, Wu YI, Loshbaugh AL, Kuhlman B, Hahn KM, Kasai H (2015) Labelling and optical erasure of synaptic memory traces in the motor cortex. Nature 525:333–338. CrossRef Medline

Hering H, Sheng M (2001) Dendritic spines: structure, dynamics and regulation. Nat Rev Neurosci 2:880–888. CrossRef Medline

Hodges JL, Yu X, Gilmore A, Bennett H, Tjia M, Perna JF, Chen CC, Li X, Lu J, Zuo Y (2017) Astrocytic contributions to synaptic and learning abnormalities in a mouse model of fragile X syndrome. Biol Psychiatry 82:139–149. CrossRef Medline

Holtmaat A, Svoboda K (2009) Experience-dependent structural synaptic plasticity in the mammalian brain. Nat Rev Neurosci 10:647–658. CrossRef Medline

Holtmaat AJ, Trachtenberg JT, Wilbrecht L, Shepherd GM, Zhang X, Knott GW, Svoboda K (2005) Transient and persistent dendritic spines in the neocortex *in vivo*. Neuron 45:279–291. CrossRef Medline

Huganir RL, Nicoll RA (2013) AMPARs and synaptic plasticity: the last 25 years. Neuron 80:704–717. CrossRef Medline

Jadhav SP, Feldman DE (2010) Texture coding in the whisker system. Curr Opin Neurobiol 20:313–318. CrossRef Medline

Jadhav SP, Wolfe J, Feldman DE (2009) Sparse temporal coding of elementary tactile features during active whisker sensation. Nat Neurosci 12:792–800. CrossRef Medline

Janesick A, Wu SC, Blumberg B (2015) Retinoic acid signaling and neuronal differentiation. Cell Mol Life Sci 72:1559–1576. CrossRef Medline

Kaeser PS, Deng L, Wang Y, Dulubova I, Liu X, Rizo J, Südhof TC (2011) RIM proteins tether Ca^{2+} channels to presynaptic active zones via a direct PDZ-domain interaction. Cell 144:282–295. CrossRef Medline

Kasai H, Matsuzaki M, Noguchi J, Yasumatsu N, Nakahara H (2003) Structure-stability-function relationships of dendritic spines. Trends Neurosci 26:360–368. CrossRef Medline

Kasai H, Fukuda M, Watanabe S, Hayashi-Takagi A, Noguchi J (2010) Structural dynamics of dendritic spines in memory and cognition. Trends Neurosci 33:121–129. CrossRef Medline

Konur S, Rabinowitz D, Fenstermaker VL, Yuste R (2003) Systematic regulation of spine sizes and densities in pyramidal neurons. J Neurobiol 56:95–112. CrossRef Medline

Lee KJ, Jung JG, Arii T, Imoto K, Rhyu IJ (2007) Morphological changes in dendritic spines of purkinje cells associated with motor learning. Neurobiol Learn Mem 88:445–450. CrossRef Medline

Maghsoodi B, Poon MM, Nam CI, Aoto J, Ting P, Chen L (2008) Retinoic acid regulates RARα-mediated control of translation in dendritic RNA granules during homeostatic synaptic plasticity. Proc Natl Acad Sci U S A 105:16015–16020. CrossRef Medline

Mark M, Ghyselinck NB, Chambon P (2009) Function of retinoic acid receptors during embryonic development. Nucl Recept Signal 7:e002. CrossRef Medline

Matsuzaki M, Ellis-Davies GC, Nemoto T, Miyashita Y, Iino M, Kasai H (2001) Dendritic spine geometry is critical for AMPA receptor expression in hippocampal CA1 pyramidal neurons. Nat Neurosci 4:1086–1092. CrossRef Medline

Misner DL, Jacobs S, Shimizu Y, de Urquiza AM, Solomin L, Perlmann T, De Luca LM, Stevens CF, Evans RM (2001) Vitamin A deprivation results in reversible loss of hippocampal long-term synaptic plasticity. Proc Natl Acad Sci U S A 98:11714–11719. CrossRef Medline

Morriss-Kay GM, Sokolova N (1996) Embryonic development and pattern formation. FASEB J 10:961–968. CrossRef Medline

Nimchinsky EA, Sabatini BL, Svoboda K (2002) Structure and function of dendritic spines. Annu Rev Physiol 64:313–353. CrossRef Medline

Nithianantharajah J, Hannan AJ (2006) Enriched environments, experience-dependent plasticity and disorders of the nervous system. Nat Rev Neurosci 7:697–709. CrossRef Medline

Nomoto M, Takeda Y, Uchida S, Mitsuda K, Enomoto H, Saito K, Choi T, Watabe AM, Kobayashi S, Masushige S, Manabe T, Kida S (2012) Dysfunction of the RAR/RXR signaling pathway in the forebrain impairs hippocampal memory and synaptic plasticity. Mol Brain 5:8. CrossRef Medline

Poon MM, Chen L (2008) Retinoic acid-gated sequence-specific translational control by RARα. Proc Natl Acad Sci U S A 105:20303–20308. CrossRef Medline

Sarti F, Schroeder J, Aoto J, Chen L (2012) Conditional RARα knock-out mice reveal acute requirement for retinoic acid and RARα in homeostatic plasticity. Front Mol Neurosci 5:16. CrossRef Medline

Sarti F, Zhang Z, Schroeder J, Chen L (2013) Rapid suppression of inhibitory synaptic transmission by retinoic acid. J Neurosci 33:11440–11450. CrossRef Medline

Schikorski T, Stevens CF (1999) Quantitative fine-structural analysis of olfactory cortical synapses. Proc Natl Acad Sci U S A 96:4107–4112. CrossRef Medline

Sheng M, Kim E (2011) The postsynaptic organization of synapses. Cold Spring Harb Perspect Biol 3:a005678. CrossRef Medline

Smith CN, Jeneson A, Frascino JC, Kirwan CB, Hopkins RO, Squire LR (2014) When recognition memory is independent of hippocampal function. Proc Natl Acad Sci U S A 111:9935–9940.

Tonegawa S, Tsien JZ, McHugh TJ, Huerta P, Blum KI, Wilson MA (1996) Hippocampal CA1-region-restricted knockout of NMDAR1 gene disrupts synaptic plasticity, place fields, and spatial learning. Cold Spring Harb Symp Quant Biol 61:225–238. CrossRef Medline

Tsien JZ, Chen DF, Gerber D, Tom C, Mercer EH, Anderson DJ, Mayford M, Kandel ER, Tonegawa S (1996) Subregion- and cell type-restricted gene knockout in mouse brain. Cell 87:1317–1326. CrossRef Medline

Veinante P, Lavallée P, Deschênes M (2000) Corticothalamic projections from layer 5 of the vibrissal barrel cortex in the rat. J Comp Neurol 424:197–204. CrossRef Medline

Wang HL, Zhang Z, Hintze M, Chen L (2011) Decrease in calcium concentration triggers neuronal retinoic acid synthesis during homeostatic synaptic plasticity. J Neurosci 31:17764–17771. CrossRef Medline

Welker C, Woolsey TA (1974) Structure of layer IV in the somatosensory neocortex of the rat: description and comparison with the mouse. J Comp Neurol 158:437–453. CrossRef Medline

Wu HP, Ioffe JC, Iverson MM, Boon JM, Dyck RH (2013) Novel, whisker-dependent texture discrimination task for mice. Behav Brain Res 237:238–242. CrossRef Medline

Xu T, Yu X, Perlik AJ, Tobin WF, Zweig JA, Tennant K, Jones T, Zuo Y (2009) Rapid formation and selective stabilization of synapses for enduring motor memories. Nature 462:915–919. CrossRef Medline

Yang G, Pan F, Gan WB (2009) Stably maintained dendritic spines are associated with lifelong memories. Nature 462:920–924. CrossRef Medline

Yee AX, Hsu YT, Chen L (2017) A metaplasticity view of the interaction between homeostatic and Hebbian plasticity. Philos Trans R Soc Lond B Biol Sci 372:20160155. CrossRef Medline

Yu X, Zuo Y (2014) Two-photon *in vivo* imaging of dendritic spines in the mouse cortex using a thinned-skull preparation. J Vis Exp 87:e51520. CrossRef Medline

Yu X, Wang G, Gilmore A, Yee AX, Li X, Xu T, Smith SJ, Chen L, Zuo Y (2013) Accelerated experience-dependent pruning of cortical synapses in ephrin-A2 knockout mice. Neuron 80:64–71. CrossRef Medline

Zhou X, Fu X, Lin C, Zhou X, Liu J, Wang L, Zhang X, Zuo M, Fan X, Li D, Sun Y (2017) Remodeling of dendritic spines in the avian vocal motor cortex following deafening depends on the basal ganglia circuit. Cereb Cortex 27:2820–2830. CrossRef Medline

Zuo Y, Lin A, Chang P, Gan WB (2005a) Development of long-term dendritic spine stability in diverse regions of cerebral cortex. Neuron 46:181–189. CrossRef Medline

Zuo Y, Yang G, Kwon E, Gan WB (2005b) Long-term sensory deprivation prevents dendritic spine loss in primary somatosensory cortex. Nature 436:261–265. CrossRef Medline